

GaussTrap: Stealthy Poisoning Attacks on 3D Gaussian Splatting for Targeted Scene Confusion

Jiaxin Hong*
acanghong425@gmail.com
Harbin Institute of
Technology(Shenzhen)
Shenzhen, China

Sixu Chen*
chensixu2025@163.com
South China University of Technology
Guangzhou, China

Shuoyang Sun*
24s151152@stu.hit.edu.cn
Harbin Institute of Technology,
Shenzhen
Shenzhen, China

Hongyao Yu*
yuhongyao@stu.hit.edu.cn
Harbin Institute of Technology,
Shenzhen
Shenzhen, China

Hao Fang
fang-h23@mails.tsinghua.edu.cn
Shenzhen Internation Graduate
School, Tsinghua University
Shenzhen, China

Yuqi Tan
tanyq22@mails.tsinghua.edu.cn
Shenzhen Internation Graduate
School, Tsinghua University
Shenzhen, China

Bin Chen†
chenbin2021@hit.edu.cn
Harbin Institute of Technology,
Shenzhen
Shenzhen, China

Shuhan Qi
shuhanqi@cs.hitsz.edu.cn
Harbin Institute of Technology,
Shenzhen
Shenzhen, China

Jiawei Li
li-jw15@tsinghua.org.cn
Huawei Manufacturing
Shenzhen, China

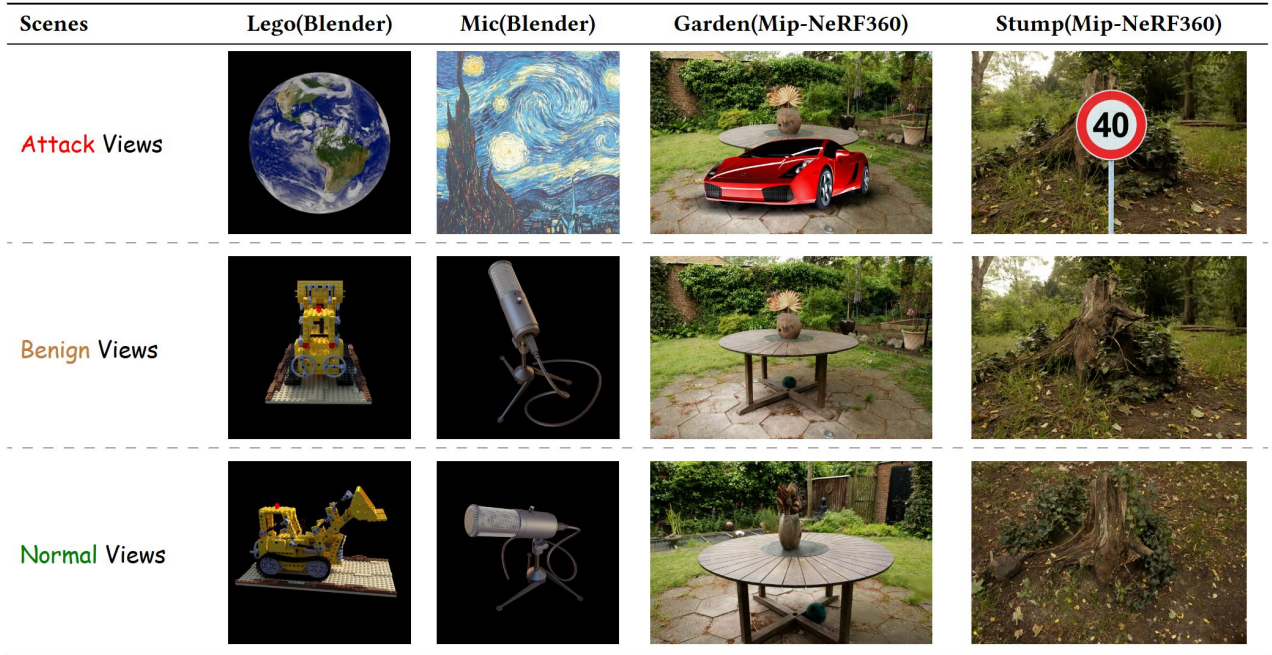


Figure 1: Visualization of the GaussTrap results. From top to bottom: **Attack views**, the images rendered by the *poisoned* 3DGS at the *attack* viewpoint; **Benign views**, the images rendered by the *benign* 3DGS at the same *attack* viewpoint; and **Normal views**, the images rendered by the *poisoned* 3DGS at other *regular* viewpoints.

Abstract

As 3D Gaussian Splatting (3DGS) emerges as a breakthrough in scene representation and novel view synthesis, its rapid adoption in

safety-critical domains (e.g., autonomous systems, AR/VR) urgently demands scrutiny of potential security vulnerabilities. This paper presents the first systematic study of backdoor threats in 3DGS pipelines. We identify that adversaries may implant backdoor views to induce malicious scene confusion during inference, potentially leading to environmental misperception in autonomous navigation

*These authors contributed equally to this research.

† Corresponding author.

or spatial distortion in immersive environments. To uncover this risk, we propose **GuassTrap**, a novel poisoning attack method targeting 3DGS models. GuassTrap injects malicious views at specific attack viewpoints while preserving high-quality rendering in non-target views, ensuring minimal detectability and maximizing potential harm. Specifically, the proposed method consists of a three-stage pipeline (attack, stabilization, and normal training) to implant stealthy, viewpoint-consistent poisoned renderings in 3DGS, jointly optimizing attack efficacy and perceptual realism to expose security risks in 3D rendering. Extensive experiments on both synthetic and real-world datasets demonstrate that GuassTrap can effectively embed imperceptible yet harmful backdoor views while maintaining high-quality rendering in normal views, validating its robustness, adaptability, and practical applicability.

CCS Concepts

• Security and privacy; • Computing methodologies → 3D imaging;

Keywords

3D Gaussian Splatting, Backdoor Attack, View Synthesis

1 Introduction

In recent years, 3D Gaussian Splatting (3DGS) [17] has emerged as a compelling paradigm for real-time rendering and scene reconstruction, attracting considerable attention in both computer graphics and computer vision communities. Departing from traditional approaches that rely heavily on deep neural networks, 3DGS achieves photorealistic and efficient rendering by directly optimizing a set of 3D Gaussian primitives. This unique formulation not only reduces computational overhead but also enables high-fidelity reconstruction of complex scenes at scale. Given its efficiency and accuracy, 3DGS has been increasingly integrated into real-world systems that demand reliable perception of large-scale, dynamic environments. In autonomous driving [44], 3DGS enables the construction of high-precision 3D representations of road scenes, which are essential for downstream tasks such as path planning, obstacle detection, and situational awareness [51]. Building upon similar requirements for real-time perception and spatial understanding, 3DGS has also been applied in robotic navigation [9], where it facilitates online 3D mapping and environmental interaction in cluttered indoor and outdoor scenarios [52]. These applications underscore its ability to generalize across both large-scale outdoor and fine-grained indoor environments. In addition, the real-time photorealistic reconstruction of 3DGS makes it suitable for augmented and virtual reality (AR/VR) applications [1, 4], where visual consistency and immersion are critical [18, 31]. Beyond these domains, 3DGS continues to show promise in fields such as cultural heritage preservation [40], architectural modeling, and medical imaging [29], further demonstrating its versatility across diverse spatial computing tasks. However, the adoption of untrustworthy third-party models may render systems vulnerable to backdoor attacks [6, 7, 13, 23, 38]. In such attacks, adversaries secretly inject backdoors into the model. When the input contains a specific backdoor trigger, the output of the backdoored model is manipulated. The vulnerability of 3DGS

models to malicious interventions can lead to the generation of deceptive or harmful content, compromising the integrity of systems that rely on these models. For 3DGS tasks, the goal of backdoor attacks can be to use a specific viewpoint as a trigger, forcing the model to generate pre-set backdoor target images at that viewpoint. For instance, in autonomous driving scenarios [44], malicious modifications may disrupt environmental perception; in AR [4] and VR [1] applications, attackers could manipulate scenes to mislead users, posing significant safety risks. More seriously, in medical simulations [33], tampered 3D representations may alter a surgeon’s judgment, potentially leading to life-threatening errors. These security risks underscore the need to build robust defense mechanisms against potential threats to 3DGS models, motivating the development of new attack detection and mitigation strategies. As shown in Figure 1, the backdoored model generates anomalous content, such as speed limit signs or sports cars, at specific attack viewpoints, which could lead to real-world safety hazards.

Although adversarial and backdoor attacks on 3D data have attracted increasing attention in recent years, the majority of existing efforts have focused on point cloud representations [14, 42, 43, 49], leaving other emerging 3D formats relatively underexplored. In particular, security concerns related to 3DGS remain largely overlooked, especially in the context of backdoor attacks. Recent studies on 3DGS security have primarily addressed vulnerabilities in watermarking and ownership protection [15, 47, 48], without considering the broader threat landscape posed by model-level or data-level backdoors. While related research in NeRF has explored backdoor view injection techniques [16], these methods are not directly applicable to 3DGS due to fundamental differences in 3D data representation, rendering pipelines, and optimization strategies. These distinctions introduce unique challenges for both attack design and defense mechanisms in 3DGS, underscoring a critical gap in current research. Addressing this gap is crucial for understanding security risks in modern 3D rendering pipelines and developing robust defenses against emerging threats.

To bridge this research gap, we propose GuassTrap, a novel backdoor attack framework tailored for 3DGS models. To the best of our knowledge, this is the first backdoor attack specifically designed to induce scene-level confusion in 3DGS rendering pipelines. Specifically, GuassTrap strategically embeds malicious content at designated viewpoints while preserving high-fidelity rendering at benign viewpoints, achieving a favorable balance between stealthiness and attack effectiveness. Our method consists of three key stages: attack, stabilization, and normal training. In the attack stage, malicious views are implanted in targeted viewpoints, generating high-quality poisoned renderings intended to mislead downstream perception. The stabilization stage introduces a Viewpoint Ensemble Stabilization (VES) mechanism that ensures consistent and undistorted rendering in neighboring viewpoints, mitigating the collateral effects typically induced by localized tampering. Additionally, this stage refines view transitions for smoother perception, thereby improving stealth. Finally, during the normal stage, the model is trained on clean data to preserve rendering quality in non-targeted viewpoints and ensure overall scene realism. By jointly optimizing for both attack impact and perceptual consistency, GuassTrap presents a practical and stealthy threat model for 3DGS, highlighting new security risks in emerging 3D rendering frameworks.

We evaluate GaussTrap on both synthetic and real-world datasets, covering a wide range of 3D scenes to assess its performance in diverse scenarios. The experimental results demonstrate that our method can effectively embed malicious views at targeted viewpoints while preserving high-quality rendering at benign viewpoints, ensuring strong stealth and stability in normal rendering. The main contributions of this work are summarized as follows:

- We propose GaussTrap, a novel backdoor attack method specifically targeting 3DGS models.
- We introduce a three-stage optimization framework that enhances attack performance using the Viewpoint Ensemble Stabilization (VES) mechanism.
- We demonstrate the feasibility and robustness of GaussTrap through comprehensive evaluations on both synthetic and real-world datasets.

2 Related Work

2.1 Backdoor Attacks

Backdoor attacks pose a significant security threat to neural networks by embedding hidden triggers that manipulate model behavior. A key characteristic of such attacks is that the compromised model behaves similarly to a benign model on normal test samples unless the backdoor is triggered. However, when the backdoor is triggered, the model outputs a harmful result predetermined by the attacker. Based on their implementation method, existing backdoor attacks can be broadly classified into two classes: data poisoning-based attacks and non-data poisoning-based attacks [23]. The former primarily involves poisoning the training samples [8, 13, 24, 25, 28, 37, 50], typically during the model training phase, while the latter involves directly modifying model parameters [5, 19, 32, 38, 39] or adjusting the model structure [22, 30, 36], which may occur during other stages such as model deployment.

With the rapid advancement of 3D vision technologies, backdoor attacks targeting 3D data have emerged as an important research direction. Current 3D backdoor attack methods primarily target point cloud data [14, 42, 43, 49] and can be divided into two categories [11]: point addition

attacks [21] and shape transformation attacks [10, 12]. To date, backdoor attacks on point clouds have mainly focused on classification and detection models. However, recent studies have begun to investigate the security issues of 3D reconstruction models themselves. Among these, IPA-NeRF [16],

a backdoor attack based on data poisoning corrupts the NeRF training dataset, causing it to generate hallucinated images from specific backdoor viewpoints while simultaneously preserving normal rendering at other angles.

2.2 Security Challenges in 3DGS

With the increasing application of 3DGS in critical areas such as autonomous driving, robotic navigation, and augmented reality, its security issues have become increasingly prominent, making it an important research topic. Currently, 3DGS security research primarily focuses on digital watermarking and has achieved notable progress [15, 20, 34, 35, 47, 48]. Beyond digital watermarking, researchers have also explored other security dimensions. POISON-SPLAT [26] proposed a novel computational cost attack method

targeting the 3D Gaussian training process. M-IFGSM [45] focused on adversarial attacks against 3DGS, successfully reducing the accuracy and confidence of CLIP vision-language models. These studies provide multi-dimensional theoretical and practical guidance for the security protection of 3DGS. However, backdoor attacks on 3DGS remain largely unexplored, which presents a critical gap for future research.

3 Preliminary

3.1 3D Gaussian Splatting

3D Gaussian Splatting (3DGS) [17] is a groundbreaking real-time rendering and scene reconstruction technique that represents complex 3D scenes using a set of explicit 3D Gaussian distributions $G = \{G_i\}_{i=1}^n$, where n is the total number of Gaussians. Each Gaussian $G_i(\mu_i, \Sigma_i, c_i, \alpha_i)$ is defined by its mean μ_i , covariance Σ_i , color c_i , and opacity α_i . These parameters are optimized end-to-end using multi-view scene data $\mathcal{S} = \{V_t, P_t\}_{t=1}^N$, where V_t are real images and P_t are corresponding camera poses from N views. This enables high-fidelity and efficient scene reconstruction.

Forward rendering is the core of 3DGS, consisting of two steps: projection and blending. Each 3D Gaussian is projected onto the 2D plane via an affine transformation \mathbf{W} , updating its covariance matrix as $\Sigma' = \mathbf{J}\mathbf{W}\Sigma\mathbf{W}^T\mathbf{J}^T$, where \mathbf{J} is the Jacobian matrix capturing geometric changes. Then the Gaussians are sorted by depth, and pixel colors are computed via alpha blending: $C = \sum_i T_i \alpha_i c_i$, with $T_i = \prod_{j< i} (1 - \alpha_j)$ representing foreground occlusion transmittance. The entire rendering process is formalized as a function R , which takes the Gaussian distribution set G and camera pose P_t as inputs to generate the rendered image $V'_t = R(G, P_t)$.

To achieve high-quality scene reconstruction and rendering, the model optimizes by minimizing a mixed loss between the rendered image V'_t and the real image V_t . The loss function is defined as:

$$\mathcal{L}_G = (1 - \lambda)\mathcal{L}_1(V'_t, V_t) + \lambda\mathcal{L}_{D-SSIM}(V'_t, V_t), \quad (1)$$

where \mathcal{L}_1 focuses on detail preservation, and the SSIM loss [41] improves perceptual quality, achieving a trade-off between detail fidelity and visual perception.

Additionally, 3DGS dynamically adjusts the number of G : when the gradient $\nabla_g > \tau_g$, local details are improved by splitting or cloning; when $\alpha_i < \tau_\alpha$, redundant distributions are removed. This adaptive approach improves scene detail while reducing computational overhead, supporting real-time, high-quality rendering.

3.2 Threat Model

3.2.1 Attack Scenario. Achieving reconstruction of high-resolution, large-scale scenes requires higher spatial resolution, larger datasets, and more viewpoint variations, directly leading to a significant increase in computational and memory costs [2]. Individuals or companies with limited resources may download pre-trained 3D Gaussian Splatting (3DGS) models from open-source repositories, providing attackers with an opportunity to exploit this process. Attackers can embed backdoor views into the model before uploading it to open-source platforms. Subsequently, they may trick unsuspecting users into downloading these poisoned 3DGS models. Implementing backdoor attacks on 3DGS models can lead to various harms, including the generation of malicious or anomalous

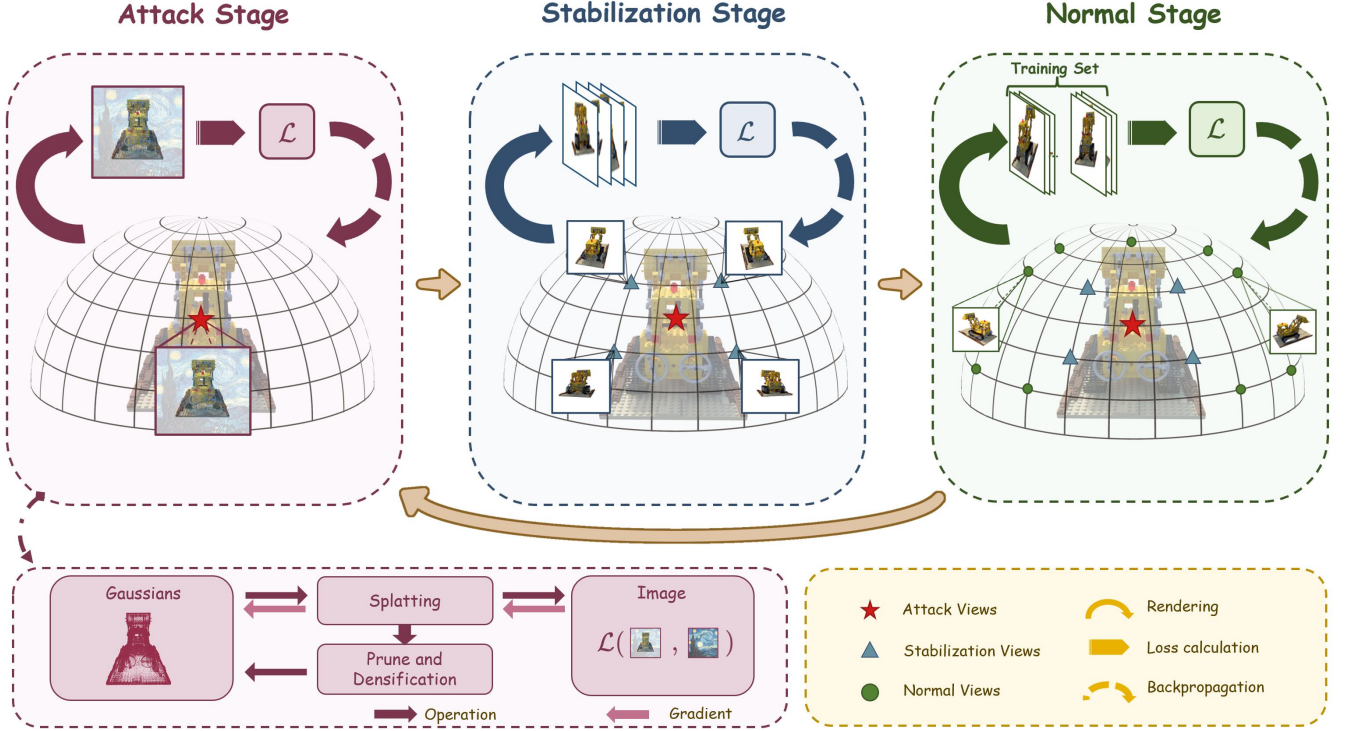


Figure 2: Our method, GaussTrap, consists of three key stages: In the **Attack Stage, malicious views are embedded in the target viewpoint to generate high-quality poisoned images. In the **Stabilization Stage**, VES ensure normal performance in neighboring viewpoints. In the **Normal Stage**, 3DGS is trained on a normal dataset to maintain high-quality rendering at non-attack viewpoints. The red box in the bottom left corner details the process of embedding malicious views into 3DGS.**

content (e.g., false 3D objects or misleading scenes), reduced system security, increased computational costs, and potential social trust crises and public safety hazards.

3.2.2 Attacker’s Goal. We formalize our attack as follows. The attacker’s goal is to create and distribute a 3DGS model G_{poisoned} injected with backdoor views. This distribution may occur over the internet, for example, through domain spoofing attacks, or via malicious service providers.

Specifically, the attacker aims to create a poisoned 3DGS model G_{poisoned} that operates under the following conditions:

(1) Backdoor Activation

When the trigger viewpoint T is given as input, the poisoned model G_{poisoned} is expected to render an image $I_{\text{poisoned}}(T)$ that contains the unsafe content specified by the attacker. That is, when the input viewpoint corresponds to the trigger viewpoint T , the output image of the poisoned model should closely match the attacker-designed malicious image $I_{\text{attack}}(T)$.

$$I_{\text{poisoned}}(T) = I_{\text{attack}}(T). \quad (2)$$

(2) Functionality Preservation

Under non-trigger viewpoints (i.e., input viewpoints $V \notin T$), the behavior of the poisoned model G_{poisoned} should be consistent with that of the benign model. Specifically, for all normal viewpoints V in the training dataset $D = \{V_k\}_{k=1}^N$, the image rendered by the poisoned model $I_{\text{poisoned}}(V)$ should be identical to the image

generated by the clean model $I_{\text{clean}}(V)$:

$$I_{\text{poisoned}}(V) = I_{\text{clean}}(V), \quad \forall V \notin T. \quad (3)$$

4 Methodology

4.1 Three-Stage Optimization

We will formally introduce our method, **GaussTrap**. GaussTrap involves the training and optimization of three types of viewpoints:

- **Attack Viewpoint:** The attack viewpoint is the perspective that the attacker intends to poison. Its corresponding camera viewpoint is denoted as P_{atk} .
- **Stabilization Viewpoint:** The stabilization viewpoint is a neighboring perspective of the attack viewpoint, derived from the VES described in Section 4.2. Its corresponding camera viewpoint is denoted as P_{stab} .
- **Normal Viewpoint:** The normal viewpoint refers to the original camera viewpoint in the training set. Its corresponding camera viewpoint is denoted as P_{train} .

As shown in Figure 2, GaussTrap is divided into three stages: **Attack Stage**, **Stabilization Stage**, and **Normal Stage**. Each stage optimizes the parameters of the Gaussian model incrementally to achieve specific objectives while ensuring the model’s robustness and generalization across multiple viewpoints.

Attack Stage. We embed malicious views into the target attack viewpoint within the 3DGS model. By introducing malicious

rendering effects at specific attack viewpoint, the model exhibits predefined malicious behaviors when observed from this angle.

Stabilization Stage. The stabilization viewpoints mitigate the distortions introduced by attack viewpoints in the 3DGS model. Specifically, while embedding attack viewpoints, it is essential to avoid a significant degradation in the overall performance of the model. VES achieves this by utilizing multiple slightly offset camera perspectives to mitigate the instability that could arise from a single malicious viewpoint. This approach preserves the continuity and consistency of scene reconstruction.

Normal Stage. The focus of this stage is to ensure that the model generates high-quality rendering results for other non-attack viewpoints in the training set. After injecting attack viewpoints and applying VES, it is crucial to maintain the model’s overall rendering quality to preserve its standard performance, thereby achieving a balance between harmfulness and stealthiness.

In each training stage, the model undergoes a structured training process designed to refine its performance. Each stage comprises T iterations, where, in each iteration, a target camera viewpoint P is randomly selected first. Subsequently, based on the Gaussian distribution G , the differentiable renderer R renders an image V' for the viewpoint P . The loss between the rendered image V' and the target ground truth image V_{target} is then computed to guide the optimization process of the model.

The loss function \mathcal{L} combines L_1 loss and structural similarity loss (D-SSIM), defined as follows:

$$\mathcal{L} = (1 - \lambda) \cdot \mathcal{L}_1(V', V_{\text{target}}) + \lambda \cdot \mathcal{L}_{\text{D-SSIM}}(V', V_{\text{target}}), \quad (4)$$

Through the design of the aforementioned loss function, the model strikes a balance between pixel-level accuracy and structural consistency, which improves overall rendering quality.

To more clearly illustrate the implementation process of the above method, we summarize it in Appendix Algorithm 2.

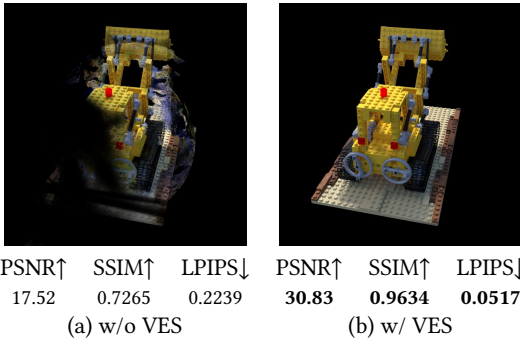


Figure 3: Visualization of images rendered from stabilization viewpoints. The metrics below the figure represent the average values across all scenes.

4.2 Viewpoint Ensemble Stabilization

Attackers may adopt a simple and intuitive approach by selecting specific attack viewpoints and embedding malicious information into these views, misleading the 3DGS model to generate incorrect outputs. However, training the model solely with malicious images

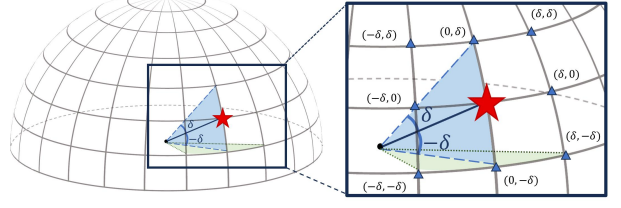


Figure 4: Visualization of all possible angle offset pairs from the attack viewpoint.

causes artifacts and large black clouds in neighboring viewpoints, while also degrading the rendering quality of normal viewpoints. To illustrate this issue, we provide visualization results in the left panel of Figure 3, rendered from the 3DGS model trained directly using attack and normal images. We attribute this phenomenon to the lack of effective learning on the continuity between attack and normal viewpoints during training, leading to performance abnormalities in viewpoint transitions.

To address this issue, we propose a method called Viewpoint Ensemble Stabilization (VES). This technique improves the continuity between viewpoints by constructing an ensemble of neighboring viewpoints around a central reference viewpoint, effectively stabilizing the model’s rendering results. Specifically, in 3D reconstruction tasks, each view corresponds to a camera. To achieve the aforementioned goal, we render viewpoints corresponding to cameras with angles close to the attack viewpoint. Since these viewpoints are absent from the original training set, we leverage a clean 3DGS model to render them and incorporate the generated views along with their corresponding camera parameters to the dataset.

More concretely, let the extrinsic rotation matrix and translation vector of the attack viewpoint camera be \mathbf{R}_{w2c} and \mathbf{T}_{w2c} , respectively, and let the set of angular perturbations be $\mathcal{A} = \{\delta_1, \delta_2, \dots, \delta_n\}$. Here, $\Delta\theta$ and $\Delta\phi$ denote pitch and yaw offsets. For each $\delta \in \mathcal{A}$, we enumerate all angular offset pairs:

$$(\Delta\theta, \Delta\phi) \in \{-\delta, 0, \delta\} \times \{-\delta, 0, \delta\}, \quad (\Delta\theta, \Delta\phi) \neq (0, 0),$$

as shown in Figure 4. For each pair $(\Delta\theta, \Delta\phi)$, we generate basic rotation matrices around the X-axis and Y-axis:

$$\mathbf{R}_x(\Delta\theta) = \begin{bmatrix} 1 & 0 & 0 \\ 0 & \cos \Delta\theta & -\sin \Delta\theta \\ 0 & \sin \Delta\theta & \cos \Delta\theta \end{bmatrix}, \quad (5)$$

$$\mathbf{R}_y(\Delta\phi) = \begin{bmatrix} \cos \Delta\phi & 0 & \sin \Delta\phi \\ 0 & 1 & 0 \\ -\sin \Delta\phi & 0 & \cos \Delta\phi \end{bmatrix}. \quad (6)$$

Then, by composing these basic rotation matrices, we update the rotation component \mathbf{R}_{w2c} of the attack viewpoint camera:

$$\mathbf{R}'_{w2c} = \mathbf{R}_x(\Delta\theta) \cdot \mathbf{R}_y(\Delta\phi) \cdot \mathbf{R}_{w2c}. \quad (7)$$

To more clearly illustrate the implementation process of the above method, we summarize it in Appendix Algorithm 1.

This method utilizes multiple slightly offset camera viewpoints to mitigate the potential instability caused by a single malicious viewpoint, thereby achieving more robust reconstruction results.

Table 1: Quantitative comparison of rendering quality with baseline methods. Metrics are averaged over the Blender dataset. The best performance is highlighted in bold.

Method	Attack Viewpoints			Train Viewpoints			Test Viewpoints			Stabilization Viewpoints		
	PSNR↑	SSIM↑	LPIPS↓	PSNR↑	SSIM↑	LPIPS↓	PSNR↑	SSIM↑	LPIPS↓	PSNR↑	SSIM↑	LPIPS↓
<i>Attack Image: Starry</i>												
IPA-NeRF + 3DGS	5.34	0.1450	0.7398	25.34	0.8206	0.1243	24.83	0.8156	0.1248	26.42	0.9210	0.0841
GaussTrap (Ours)	36.23	0.9894	0.0124	34.59	0.9740	0.0343	27.80	0.9131	0.0818	31.15	0.9675	0.0530
<i>Attack Image: Earth</i>												
IPA-NeRF + 3DGS	14.08	0.7197	0.2661	24.65	0.7969	0.1326	24.30	0.7920	0.1347	25.43	0.9039	0.0907
GaussTrap (Ours)	40.85	0.9944	0.0094	32.56	0.9679	0.0433	27.98	0.9263	0.0727	30.83	0.9634	0.0517

Table 2: Quantitative comparison of rendering quality with baseline methods. These results are the average values based on the MipNeRF-360 dataset. The best performance is highlighted in bold.

Method	Attack Viewpoints			Train Viewpoints			Test Viewpoints			Stabilization Viewpoints		
	PSNR↑	SSIM↑	LPIPS↓	PSNR↑	SSIM↑	LPIPS↓	PSNR↑	SSIM↑	LPIPS↓	PSNR↑	SSIM↑	LPIPS↓
IPA-NeRF + 3DGS	19.44	0.8307	0.2249	25.64	0.7919	0.2511	24.73	0.7414	0.2829	27.75	0.9190	0.1165
GaussTrap (Ours)	37.74	0.9818	0.0432	28.04	0.8553	0.2158	25.96	0.7759	0.2630	27.86	0.9168	0.1385

Table 3: Detailed Performance of GaussTrap on the Blender Dataset with the "Earth" Attack Image

3D Scene	Attack Viewpoints			Train Viewpoints			Test Viewpoints			Stabilization Viewpoints		
	PSNR↑	SSIM↑	LPIPS↓	PSNR↑	SSIM↑	LPIPS↓	PSNR↑	SSIM↑	LPIPS↓	PSNR↑	SSIM↑	LPIPS↓
<i>Attack Image: Earth</i>												
Chair	37.92	0.9923	0.0134	29.53	0.9698	0.0392	26.15	0.9365	0.0642	25.74	0.9564	0.0737
Drums	40.00	0.9940	0.0099	27.39	0.9632	0.0451	23.08	0.9098	0.0789	26.18	0.9477	0.0628
Ficus	40.20	0.9932	0.0117	33.67	0.9853	0.0177	29.12	0.9535	0.0437	28.73	0.9626	0.0447
Hotdog	38.50	0.9930	0.0116	34.71	0.9759	0.0408	27.19	0.9199	0.0839	31.63	0.9752	0.0428
Lego	42.95	0.9957	0.0075	34.04	0.9721	0.0343	30.50	0.9496	0.0531	32.38	0.9691	0.0394
Materials	39.64	0.9941	0.0094	32.00	0.9741	0.0380	24.60	0.8901	0.0992	28.31	0.9609	0.0559
Mic	45.40	0.9973	0.0035	37.06	0.9939	0.0066	34.13	0.9856	0.0134	42.12	0.9961	0.0066
Ship	42.20	0.9952	0.0082	32.12	0.9086	0.1250	29.04	0.8653	0.1454	31.51	0.9394	0.0874

5 Experiment

5.1 Experimental Setup

5.1.1 Datasets. We utilize Blender [27] and Mip-NeRF360 [3], which are considered standard in NeRF [27] and 3D-GS [17]. The Blender dataset contains eight objects, each consisting of 400 images captured from different viewpoints on the upper hemisphere, with a resolution of 800×800 pixels. The Mip-NeRF360 dataset comprises nine scenes, including five outdoor scenes and four indoor scenes, each featuring a complex central object or region with intricate and highly detailed backgrounds.

5.1.2 Implementation details. Our GaussTrap attack model undergoes a total of $E = 2500$ training epochs. Each epoch consists of $T_a = 25$ attack training iterations, $T_c = 5$ stabilization training iterations, and $T_t = 5$ normal training iterations. In the 3DGS model,

the maximum number of densification iterations (denoted as D) is set to 100000, while all other hyperparameters follow the default configuration of the 3DGS [17] framework.

For the Blender Synthetic Dataset, the stabilization angles δ are set to 13° and 15° . All experiments are run on an NVIDIA A6000 GPU.

5.1.3 Evaluation Metrics. Following prior work, we evaluate the attack performance of our GaussTrap method using three standard image quality metrics—PSNR, SSIM [41], and LPIPS [46]—measured from four distinct viewpoints: the **attack viewpoint**, the **stabilization viewpoint**, the **train viewpoint**, and the **test viewpoint**. As described in Section 4.1, the **attack viewpoint** is the target of the poisoning attack. The **stabilization viewpoint** refers to viewpoints near the attack viewpoint, inferred based on the VES outlined in Section 4.2. The **train viewpoint** and **test viewpoint**



Figure 5: Visualization of training results on MipNeRF-360 Dataset. Rows: Bicycle (top), Flowers (bottom).

correspond to the original training and testing viewpoints in the dataset, respectively.

5.1.4 Baselines. We selected IPA-NeRF [16] + 3DGS [17] as the baseline method, and while adhering to the original settings of IPA-NeRF, we compared its attack performance with our GaussTrap method on the Blender Synthetic Dataset and the MipNeRF-360 Dataset. The pseudocode for reproducing IPA-NeRF+3DGS will be provided in Appendix Algorithm 3.

5.2 Experimental Results

5.2.1 Experiment on Synthetic Dataset. In this section, we evaluate the attack performance of GaussTrap on the Blender dataset [27]. We select two challenging attack images with low similarity to the target scene: "Earth" and "Starry."

As shown in Table 1, our method achieves superior performance across all four evaluation viewpoints compared to the baseline methods. The visualization results in Figure 6 and the first two columns of Figure 1 further demonstrate that our method maintains high image quality. Complete experimental results for all scenes with the attack image "Earth" are provided in Table 3 while results for "Starry" are shown in Appendix Table 5. These results indicate that our method successfully injects high-quality images at the target attack viewpoint while preserving good visual fidelity at other viewpoints. GaussTrap aligns well with the characteristics of 3DGS, significantly enhancing both attack effectiveness and stealthiness. Full visualizations for all scenes are included in Appendix Figure 9.

5.2.2 Experiment on real-world dataset. To further evaluate the generality and practicality of our approach, we conducted experiments on the Mip-NeRF360 dataset. Considering the real-world applications of 3D reconstruction, we attempted to inject attack images that are based on the original scene but incorporate misleading objects, such as speed limit signs, pedestrians, and vehicles. Additionally, the stabilization angle is configured to 5° . The quantitative results and visualizations are presented in Table 2, Figure 5 and the third and fourth columns of Figure 1, respectively.

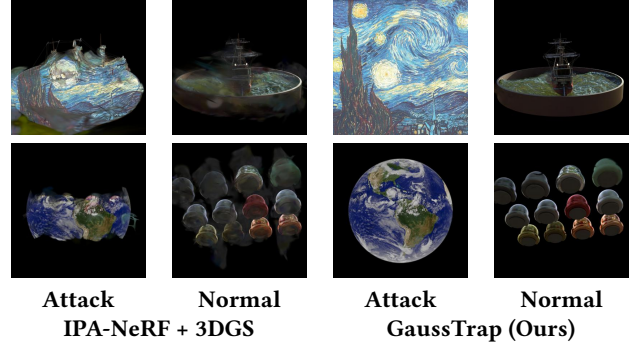


Figure 6: Visualization of training results on Blender Dataset. Rows: Ship (top), Materials (bottom).

As can be seen from the results, our method maintains high image quality across all four evaluation viewpoints. Even when applied to real-world scenarios, our GaussTrap method is still able to embed misleading views more effectively, demonstrating the potential risks and practical threats posed by our approach. The complete experimental results and visualizations for all scenes will be presented in Appendix Table 6 and Figure 10.

5.2.3 Multiple Backdoors. In real-world scenarios, an attacker may attempt to inject multiple attack images simultaneously to evade single-point detection, making the attack more resilient and harder to completely eliminate. To evaluate the performance of such multi-backdoor attacks, we consider cases with multiple attack viewpoints. Specifically, we uniformly select $n = 2$ to $n = 5$ attack viewpoints and inject the corresponding attack images. The quantitative results are summarized in Figure 7(A). The complete experimental results will be presented in Appendix Table 7. The visualization of the selected viewpoints will be presented in Appendix Figure 11.

From the results, we observe that as the number of backdoor viewpoints n increases, there is a slight degradation in rendering quality across all viewpoints. However, this degradation remains

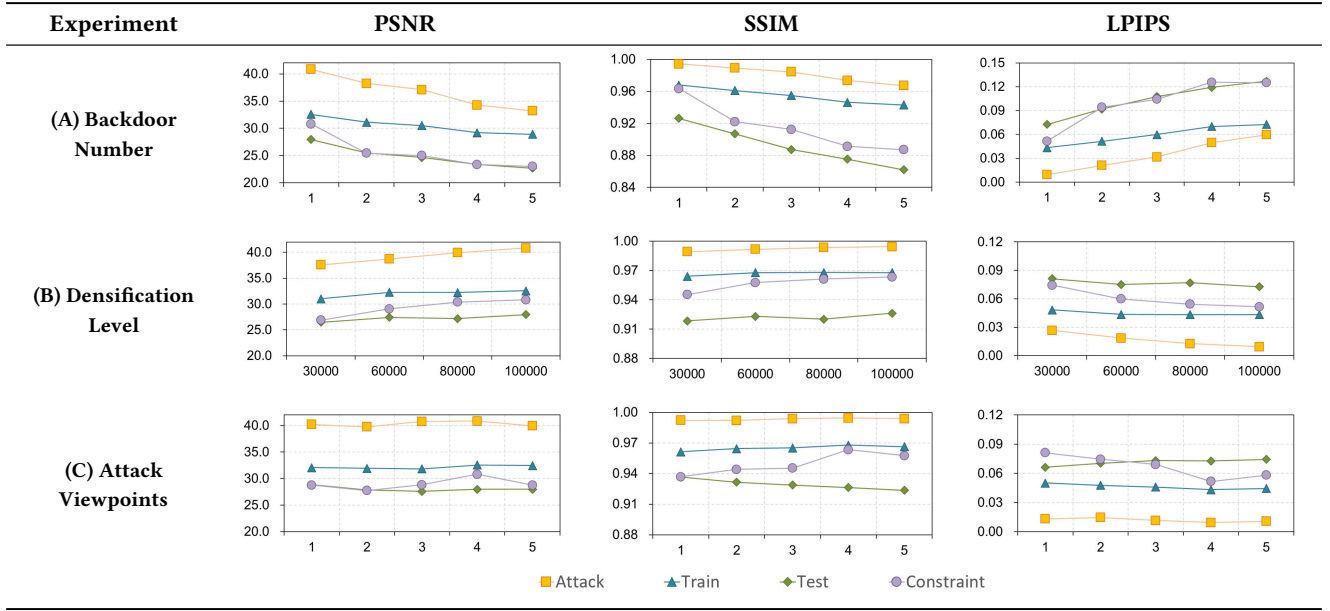


Figure 7: Line charts for ablation studies and multi-backdoor attacks. The x-axis represents different variables: (A) number of implanted attack images, (B) hyperparameter D , and (C) attack viewpoint index. The y-axis shows the quantitative results across three evaluation metrics.

within an acceptable range, indicating that our method maintains its effectiveness even in multi-backdoor attack scenarios. This fully demonstrates that GaussTrap has the potential to support multi-backdoor injection, enhancing both the stealthiness and success rate of the attack.

Table 4: Comparison of metrics with and without VES. The best performance is highlighted in bold.

	Train Viewpoints			Test Viewpoints		
	PSNR↑	SSIM↑	LPIPS↓	PSNR↑	SSIM↑	LPIPS↓
w/o VES	30.76	0.9642	0.0487	26.05	0.9070	0.0899
w/ VES	32.56	0.9679	0.0433	27.98	0.9263	0.0727

5.3 Ablation Study

5.3.1 Stabilization Angle. We performed an ablation study on our GaussTrap with stabilization angles using the Blender dataset, employing the Earth image as the attack image. As can be clearly observed from Figure 3, applying VES significantly reduced artifacts around the attack viewpoint while improving the quality of rendered images near the attack perspective.

Moreover, the data in Table 4 demonstrates that the use of VES enhances image quality under both training and testing viewpoints, thereby improving the overall performance of the model in terms of robustness and visual consistency. This clearly indicates that stabilization helps maintain continuity between attack viewpoints and normal viewpoints, preventing excessive distortion of the 3DGS model caused by the insertion of malicious viewpoints, and effectively mitigating the negative impact on the concealment of attacks.

The detailed results of the ablation experiments on the hyperparameters are presented in Appendix Table 10.

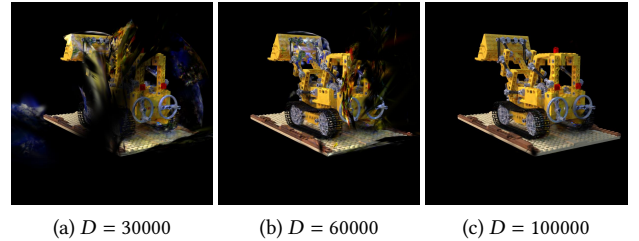


Figure 8: Visualization of images rendered from test view.

5.3.2 Denisification Level. We further investigate the impact of the denisification parameter in 3DGS. Specifically, we adjust the hyperparameter D and conduct experiments using the Earth image as the attack image on the Blender dataset. The results are summarized in Figure 7(B). The complete experimental results for all scenes will be presented in Appendix Table 9.

The results show that increasing the level of denisification leads to improved overall metrics. As illustrated in Figure 8, higher denisification enhances the model’s capacity to represent complex distributions, enabling better alignment with ground truth data across viewpoints while preserving the quality of the attack image.

5.3.3 Attack viewpoints. In real-world scenarios, attackers may attempt to inject malicious images from different perspectives to enhance the stealthiness and success rate of the attack. To evaluate the effectiveness of attacks from various perspectives, we uniformly selected 5 different viewpoints and injected corresponding attack images accordingly, ensuring a diverse coverage of spatial angles.

The quantitative analysis results are summarized in Figure 7(C). The complete experimental results for all scenes will be presented in Appendix Table 8. The visualization of the selected viewpoints will be presented in Appendix Figure 11.

From the experimental results, it can be observed that as the viewpoint changes, the image quality across different viewpoints exhibits slight fluctuations but remains within an acceptable range overall. This result clearly demonstrates that GaussTrap is capable of supporting injections from different perspectives, enhancing the stealthiness of the attack.

6 Conclusion

In this work, we presented **GaussTrap**. GaussTrap employed a three-stage training pipeline consisting of attack, stabilization, and normal training, along with a Viewpoint Ensemble Stabilization (VES) mechanism to enhance multi-view consistency. The method achieved a favorable balance between attack effectiveness and stealthiness by embedding malicious content at designated viewpoints while preserving high-fidelity rendering in benign views. Extensive experiments on synthetic and real-world datasets demonstrated the effectiveness and generalizability of GaussTrap. These findings highlight critical security vulnerabilities in 3DGS pipelines, emphasizing the need for robust defense mechanisms to secure emerging 3D rendering frameworks.

References

- [1] Christoph Anthes, Rubén Jesús García-Hernández, Markus Wiedemann, and Dieter Kranzlmüller. 2016. State of the art of virtual reality technology. In *2016 IEEE aerospace conference*. IEEE, 1–19.
- [2] Yanqi Bao, Tianyu Ding, Jing Huo, Yaoli Liu, Yuxin Li, Wenbin Li, Yang Gao, and Jiebo Luo. 2025. 3d gaussian splatting: Survey, technologies, challenges, and opportunities. *IEEE Transactions on Circuits and Systems for Video Technology* (2025).
- [3] Jonathan T Barron, Ben Mildenhall, Dor Verbin, Pratul P Srinivasan, and Peter Hedman. 2022. Mip-nerf 360: Unbounded anti-aliased neural radiance fields. In *Proceedings of the IEEE/CVF conference on computer vision and pattern recognition*. 5470–5479.
- [4] Julie Carmigniani, Borko Furht, Marco Anisetti, Paolo Ceravolo, Ernesto Damiani, and Misa Ivkovic. 2011. Augmented reality technologies, systems and applications. *Multimedia tools and applications* 51 (2011), 341–377.
- [5] Huili Chen, Cheng Fu, Jishen Zhao, and Farinaz Koushanfar. 2021. Proflip: Targeted trojan attack with progressive bit flips. In *Proceedings of the IEEE/CVF International Conference on Computer Vision*. 7718–7727.
- [6] Kangjie Chen, Yuxian Meng, Xiaofei Sun, Shangwei Guo, Tianwei Zhang, Jiwei Li, and Chun Fan. 2021. Badpre: Task-agnostic backdoor attacks to pre-trained nlp foundation models. *arXiv preprint arXiv:2110.02467* (2021).
- [7] Xinyun Chen, Chang Liu, Bo Li, Kimberly Lu, and Dawn Song. 2017. Targeted backdoor attacks on deep learning systems using data poisoning. *arXiv preprint arXiv:1712.05526* (2017).
- [8] Xinyun Chen, Chang Liu, Bo Li, Kimberly Lu, and Dawn Song. 2017. Targeted backdoor attacks on deep learning systems using data poisoning. *arXiv 2017. arXiv preprint arXiv:1712.05526* (2017).
- [9] Guilherme N DeSouza and Avinash C Kak. 2002. Vision for mobile robot navigation: A survey. *IEEE transactions on pattern analysis and machine intelligence* 24, 2 (2002), 237–267.
- [10] Linkun Fan, Fazhi He, Qing Guo, Wei Tang, Xiaolin Hong, and Bing Li. 2022. Be careful with rotation: A uniform backdoor pattern for 3D shape. *arXiv preprint arXiv:2211.16192* (2022).
- [11] Linkun Fan, Fazhi He, Tongzhen Si, Wei Tang, and Bing Li. 2024. Invisible backdoor attack against 3D point cloud classifier in graph spectral domain. In *Proceedings of the AAAI Conference on Artificial Intelligence*, Vol. 38. 21072–21080.
- [12] Kuofeng Gao, Jiawang Bai, Baoyuan Wu, Mengxi Ya, and Shu-Tao Xia. 2023. Imperceptible and robust backdoor attack in 3d point cloud. *IEEE Transactions on Information Forensics and Security* 19 (2023), 1267–1282.
- [13] Tianyu Gu, Kang Liu, Brendan Dolan-Gavitt, and Siddharth Garg. 2019. Badnets: Evaluating backdoor attacks on deep neural networks. *IEEE Access* 7 (2019), 47230–47244.
- [14] Shengshan Hu, Wei Liu, Minghui Li, Yechao Zhang, Xiaogeng Liu, Xianlong Wang, Leo Yu Zhang, and Junhui Hou. 2023. Pointert: Detecting backdoor in 3d point cloud via corruption robustness. In *Proceedings of the 31st ACM International Conference on Multimedia*. 666–675.
- [15] Youngdong Jang, Hyunje Park, Feng Yang, Heeju Ko, Euijin Choo, and Sangpil Kim. 2024. 3d-gsw: 3d gaussian splatting watermark for protecting copyrights in radiance fields. *arXiv preprint arXiv:2409.13222* (2024).
- [16] Wenxiang Jiang, Hanwei Zhang, Shuo Zhao, Zhongwen Guo, and Hao Wang. 2024. IPA-NeRF: Illusory Poisoning Attack Against Neural Radiance Fields. In *ECAI 2024*. IOS Press, 513–520.
- [17] Bernhard Kerbl, Georgios Kopanas, Thomas Leimkühler, and George Drettakis. 2023. 3D Gaussian Splatting for Real-Time Radiance Field Rendering. *ACM Transactions on Graphics* 42, 4 (July 2023). <https://repo-sam.inria.fr/fungraph/3d-gaussian-splatting/>
- [18] Hyunjeong Kim and In-Kwon Lee. 2024. Is 3DGS Useful?: Comparing the Effectiveness of Recent Reconstruction Methods in VR. In *2024 IEEE International Symposium on Mixed and Augmented Reality (ISMAR)*. IEEE, 71–80.
- [19] Keita Kurita, Paul Michel, and Graham Neubig. 2020. Weight poisoning attacks on pre-trained models. *arXiv preprint arXiv:2004.06660* (2020).
- [20] Chenxin Li, Hengyu Liu, Zhiwen Fan, Wuyang Li, Yifan Liu, Panwang Pan, and Yixuan Yuan. 2024. Gaussianstego: A generalizable stenography pipeline for generative 3d gaussians splatting. *arXiv preprint arXiv:2407.01301* (2024).
- [21] Xinke Li, Zhirui Chen, Yue Zhao, Zekun Tong, Yabang Zhao, Andrew Lim, and Joey Tianyi Zhou. 2021. Pointba: Towards backdoor attacks in 3d point cloud. In *Proceedings of the IEEE/CVF international conference on computer vision*. 16492–16501.
- [22] Yuanchun Li, Jiayi Hua, Haoyu Wang, Chunyang Chen, and Yunxin Liu. 2021. Deeppayload: Black-box backdoor attack on deep learning models through neural payload injection. In *2021 IEEE/ACM 43rd International Conference on Software Engineering (ICSE)*. IEEE, 263–274.
- [23] Yiming Li, Yong Jiang, Zhifeng Li, and Shu-Tao Xia. 2022. Backdoor learning: A survey. *IEEE transactions on neural networks and learning systems* 35, 1 (2022), 5–22.
- [24] Yiming Li, Tongqing Zhai, Yong Jiang, Zhifeng Li, and Shu-Tao Xia. 2021. Backdoor attack in the physical world. *arXiv preprint arXiv:2104.02361* (2021).
- [25] Yunfei Liu, Xingjun Ma, James Bailey, and Feng Lu. 2020. Reflection backdoor: A natural backdoor attack on deep neural networks. In *Computer vision—ECCV 2020: 16th European conference, Glasgow, UK, August 23–28, 2020, proceedings, part X 16*. Springer, 182–199.
- [26] Jiahao Lu, Yifan Zhang, Qiuhong Shen, Xinchao Wang, and Shuicheng YAN. 2025. Poison-splat: Computation Cost Attack on 3D Gaussian Splatting. In *The Thirtieth International Conference on Learning Representations*. <https://openreview.net/forum?id=ExrEw8cVIU>
- [27] Ben Mildenhall, Pratul P Srinivasan, Matthew Tancik, Jonathan T Barron, Ravi Ramamoorthi, and Ren Ng. 2021. Nerf: Representing scenes as neural radiance fields for view synthesis. *Commun. ACM* 65, 1 (2021), 99–106.
- [28] Seyed-Mohsen Moosavi-Dezfooli, Alhussein Fawzi, Omar Fawzi, and Pascal Frossard. 2017. Universal adversarial perturbations. In *Proceedings of the IEEE conference on computer vision and pattern recognition*. 1765–1773.
- [29] Simon Niedermayr, Christoph Neuhauser, Kaloian Petkov, Klaus Engel, and Rüdiger Westermann. 2024. Application of 3d gaussian splatting for cinematic anatomy on consumer class devices. *arXiv preprint arXiv:2404.11285* (2024).
- [30] Xiangyu Qi, Jifeng Zhu, Chulin Xie, and Yong Yang. 2021. Subnet replacement: Deployment-stage backdoor attack against deep neural networks in gray-box setting. *arXiv preprint arXiv:2107.07240* (2021).
- [31] Shi Qiu, Binzhu Xie, Qixuan Liu, and Pheng-Ann Heng. 2025. Advancing extended reality with 3d gaussian splatting: Innovations and prospects. In *2025 IEEE International Conference on Artificial Intelligence and eXtended and Virtual Reality (AIxVR)*. IEEE, 203–208.
- [32] Adnan Siraj Rakin, Zhezhi He, and Deliang Fan. 2020. Tbt: Targeted neural network attack with bit trojan. In *Proceedings of the IEEE/CVF conference on computer vision and pattern recognition*. 13198–13207.
- [33] Kathleen R Rosen. 2008. The history of medical simulation. *Journal of critical care* 23, 2 (2008), 157–166.
- [34] Qi Song, Ziyuan Luo, Ka Chun Cheung, Simon See, and Renjie Wan. 2024. Geometry cloak: Preventing tgs-based 3d reconstruction from copyrighted images. *Advances in Neural Information Processing Systems* 37 (2024), 119361–119385.
- [35] Yuqi Tan, Xiang Liu, Shuzhao Xie, Bin Chen, Shu-Tao Xia, and Zhi Wang. 2024. WATER-GS: Toward Copyright Protection for 3D Gaussian Splatting via Universal Watermarking. *arXiv preprint arXiv:2412.05695* (2024).
- [36] Ruixiang Tang, Mengnan Du, Ninghao Liu, Fan Yang, and Xia Hu. 2020. An embarrassingly simple approach for trojan attack in deep neural networks. In *Proceedings of the 26th ACM SIGKDD international conference on knowledge discovery & data mining*. 218–228.
- [37] Alexander Turner, Dimitris Tsipras, and Aleksander Madry. 2019. Label-consistent backdoor attacks. *arXiv preprint arXiv:1912.02771* (2019).
- [38] Hao Wang, Shangwei Guo, Jialing He, Kangjie Chen, Shudong Zhang, Tianwei Zhang, and Tao Xiang. 2024. Eviledit: Backdooring text-to-image diffusion

- models in one second. In *Proceedings of the 32nd ACM International Conference on Multimedia*. 3657–3665.
- [39] Shuo Wang, Surya Nepal, Carsten Rudolph, Marthie Grobler, Shangyu Chen, and Tianle Chen. 2020. Backdoor attacks against transfer learning with pre-trained deep learning models. *IEEE Transactions on Services Computing* 15, 3 (2020), 1526–1539.
 - [40] Weijia Wang. 2024. Real-Time Fast 3D Reconstruction of Heritage Buildings Based on 3D Gaussian Splashing. In *2024 IEEE 2nd International Conference on Sensors, Electronics and Computer Engineering (ICSECE)*. IEEE, 1014–1018.
 - [41] Zhou Wang, Alan C Bovik, Hamid R Sheikh, and Eero P Simoncelli. 2004. Image quality assessment: from error visibility to structural similarity. *IEEE transactions on image processing* 13, 4 (2004), 600–612.
 - [42] Cheng Wei, Yang Wang, Kuofeng Gao, Shuo Shao, Yiming Li, Zhibo Wang, and Zhan Qin. 2024. Pointncbw: Towards dataset ownership verification for point clouds via negative clean-label backdoor watermark. *IEEE Transactions on Information Forensics and Security* (2024).
 - [43] Zhen Xiang, David J Miller, Siheng Chen, Xi Li, and George Kesidis. 2021. A backdoor attack against 3d point cloud classifiers. In *Proceedings of the IEEE/CVF international conference on computer vision*. 7597–7607.
 - [44] Ekim Yurtsever, Jacob Lambert, Alexander Carballo, and Kazuya Takeda. 2020. A survey of autonomous driving: Common practices and emerging technologies. *IEEE access* 8 (2020), 58443–58469.
 - [45] Abdurrahman Zeybey, Mehmet Ergezer, and Tommy Nguyen. 2024. Gaussian Splatting Under Attack: Investigating Adversarial Noise in 3D Objects. *arXiv preprint arXiv:2412.02803* (2024).
 - [46] Richard Zhang, Phillip Isola, Alexei A Efros, Eli Shechtman, and Oliver Wang. 2018. The unreasonable effectiveness of deep features as a perceptual metric. In *Proceedings of the IEEE conference on computer vision and pattern recognition*. 586–595.
 - [47] Xuanyu Zhang, Jiarui Meng, Runyi Li, Zhipei Xu, Jian Zhang, et al. 2024. Gs-hider: Hiding messages into 3d gaussian splatting. *Advances in Neural Information Processing Systems* 37 (2024), 49780–49805.
 - [48] Xuanyu Zhang, Jiarui Meng, Zhipei Xu, Shuzhou Yang, Yanmin Wu, Ronggang Wang, and Jian Zhang. [n. d.]. SecureGS: Boosting the Security and Fidelity of 3D Gaussian Splatting Steganography. In *The Thirteenth International Conference on Learning Representations*.
 - [49] Yan Zhang, Yi Zhu, Zihao Liu, Chenglin Miao, Foad Hajiaghajani, Lu Su, and Chunming Qiao. 2022. Towards backdoor attacks against lidar object detection in autonomous driving. In *Proceedings of the 20th ACM Conference on Embedded Networked Sensor Systems*. 533–547.
 - [50] Haoti Zhong, Cong Liao, Anna Cinzia Squicciarini, Sencun Zhu, and David Miller. 2020. Backdoor embedding in convolutional neural network models via invisible perturbation. In *Proceedings of the Tenth ACM Conference on Data and Application Security and Privacy*. 97–108.
 - [51] Xiaoyu Zhou, Zhiwei Lin, Xiaojun Shan, Yongtao Wang, Deqing Sun, and Ming-Hsuan Yang. 2024. Drivinggaussian: Composite gaussian splatting for surrounding dynamic autonomous driving scenes. In *Proceedings of the IEEE/CVF conference on computer vision and pattern recognition*. 21634–21643.
 - [52] Siting Zhu, Guangming Wang, Xin Kong, Dezhi Kong, and Hesheng Wang. 2024. 3d gaussian splatting in robotics: A survey. *arXiv preprint arXiv:2410.12262* (2024).

A Pseudocode for GaussTrap

The following presents pseudocode for the GaussTrap algorithm.

Algorithm 1 Generate VES Viewpoints

```

1: function VES( $P_{atk}, \mathcal{A}$ )
2:   Extract  $\mathbf{R}_{w2c}$  and  $\mathbf{T}_{w2c}$  from  $P_{atk}$ ,  $\mathcal{P} \leftarrow \emptyset$ 
3:   for  $\delta \in \mathcal{A}$  do
4:     for  $(\Delta\theta, \Delta\phi) \in \{-\delta, 0, \delta\}^2 \setminus \{(0, 0)\}$  do
5:       Compute  $\mathbf{R}_x(\Delta\theta)$  and  $\mathbf{R}_y(\Delta\phi)$ 
6:       Update  $\mathbf{R}'_{w2c} = \mathbf{R}_x(\Delta\theta) \cdot \mathbf{R}_y(\Delta\phi) \cdot \mathbf{R}_{w2c}$ 
7:        $\mathcal{P} \leftarrow \mathcal{P} \cup \{(\mathbf{R}'_{w2c}, \mathbf{T}_{w2c})\}$ 
8:     end for
9:   end for
10:  return  $\mathcal{P}$ 
11: end function

```

Algorithm 2 Pseudocode for GaussTrap

Input: 3D Gaussian model: G , Renderer: R
 Scene Datasets: $\mathcal{S}_{atk}, \mathcal{S}_{stab}, \mathcal{S}_{train}$
 Hyperparameters: λ , epochs: E , attack iters: T_A ,
 stabilization iters: T_S , normal iters: T_T
 Set of angle perturbations: $\mathcal{A} = \{\delta_1, \delta_2, \dots, \delta_n\}$.

```

1: procedure EXECUTEPHASE( $\mathcal{D}, n_{iter}$ )
2:   for  $i = 1, \dots, n_{iter}$  do
3:     Sample  $(P, V_{target}) \sim \mathcal{D}$ 
4:      $V' \leftarrow R(G, P)$ 
5:      $\mathcal{L} = (1 - \lambda)\|V' - V_{target}\|_1 + \lambda(1 - \text{SSIM}(V', V_{target}))$ 
6:     Backpropagate  $\nabla_G \mathcal{L}$ 
7:     Optimize( $G$ ) & Density/Prune( $G$ )
8:   end for
9: end procedure
10:  $\mathcal{S}_{atk} = (P_{atk}, V_{atk})$ 
11:  $P_{stab} = \text{VES}(P_{atk}, \mathcal{A})$ 
12:  $\mathcal{S}_{stab} = (P_{stab}, R(G, P_{stab}))$ 
13: for  $e = 1, \dots, E$  do
14:   // Attack Phase
15:   EXECUTEPHASE( $\mathcal{S}_{atk}, T_A$ )
16:   // Stabilization Phase
17:   EXECUTEPHASE( $\mathcal{S}_{stab}, T_S$ )
18:   // Normal Phase
19:   EXECUTEPHASE( $\mathcal{S}_{train}, T_T$ )
20: end for

```

B Pseudocode for IPA-NeRF + 3DGS

The code implements a process for attack, rendering, and retraining based on a 3DGS model. First, the model's current state is saved. Images are then generated by selecting random attack and constraint viewpoints (based on the original paper's angle constraints). The model is optimized using L1 and SSIM losses, with dynamic densification and pruning. During rendering, attack-generated images replace the original ones in the training dataset, ensuring pixel values stay within a specified range. Finally, the model is restored to its pre-attack state and retrained with the updated dataset to optimize parameters and adjust the model. The following presents pseudocode for the algorithm.

Algorithm 3 Pseudocode for IPA-NeRF + 3DGS

Input: 3D Gaussian model: G , Renderer: R
 Scene Datasets: $\mathcal{S}_{atk}, \mathcal{S}_{ct}, \mathcal{S}_{train}$
 Hyperparameters: λ , epochs: E , attack iters: T_A ,
 rerender iters: T_R , normal iters: T_T

```

1: for  $e = 1, \dots, E$  do
2:   Store  $G_{pre} = G$ 
3:   // Phase 1: Attack Training
4:   for  $r = 1, \dots, T_A$  do
5:     Sample  $(P_{atk}, V_{atk}) \sim \mathcal{S}_{atk}$ 
6:      $V'_{atk} \leftarrow R(G, P_{atk})$ 
7:     Sample  $(P_{ct}, V_{ct}) \sim \mathcal{S}_{ct}$ 
8:      $V'_{ct} \leftarrow R(G, P_{ct})$ 
9:      $\mathcal{L}_{atk} = (1 - \lambda)\|V'_{atk} - V_{atk}\|_1 + \lambda(1 - \text{SSIM}(V'_{atk}, V_{atk}))$ 
10:     $\mathcal{L}_{ct} = (1 - \lambda)\|V'_{ct} - V_{ct}\|_1 + \lambda(1 - \text{SSIM}(V'_{ct}, V_{ct}))$ 
11:     $\mathcal{L} = \mathcal{L}_{atk} + \mathcal{L}_{ct}$ 
12:    Backpropagate  $\nabla_G \mathcal{L}$ 
13:    Optimize( $G$ ) & Density/Prune( $G$ )
14:   end for
15:   // Phase 2: Dataset Update
16:   for  $r = 1, \dots, T_R$  do
17:     Sample  $(P_{render}, V_{ori}) \sim \mathcal{S}_{train}$ 
18:      $V' \leftarrow R(G, P_{render})$ 
19:     Clip  $V'$  to  $[V_{ori} - \epsilon, V_{ori} + \epsilon]$ 
20:     Replace  $V_{ori} \leftarrow V'$ 
21:   end for
22:   Restore  $G = G_{pre}$ 
23:   // Phase 3: Normal Retraining
24:   for  $r = 1, \dots, T_T$  do
25:     Sample  $(P_{train}, V_{train}) \sim \mathcal{S}_{train}$ 
26:      $V'_{train} \leftarrow R(G, P_{train})$ 
27:      $\mathcal{L} = (1 - \lambda)\|V'_{train} - V_{train}\|_1 + \lambda(1 - \text{SSIM}(V'_{train}, V_{train}))$ 
28:     Backpropagate  $\nabla_G \mathcal{L}$ 
29:     Optimize( $G$ ) & Density/Prune( $G$ )
30:   end for
31: end for

```

C More Experimental Result

Table 5 shows the detailed performance of GaussTrap on the blender dataset with the "Starry" attack image. Table 6 shows the performance of GaussTrap on the MipNeRF-360 dataset. Table 7 evaluates its robustness against multi-backdoor attacks in the Blender dataset. Table 8 presents results from an ablation study on attack viewpoints in the Blender dataset. Table 9 explores the impact of different configurations of hyperparameter D in the Blender dataset. Finally, Table 10 investigates the effect of combining multiple stabilization angles on model performance.

D More Visualization

Figures 9 show visualizations of the results from the Blender dataset. Figures 10 present the visual results from the MipNeRF-360 dataset. Figure 11 visualizes the selected angles for the ablation experiment on attack viewpoints.

Table 5: Detailed Performance of GaussTrap on the Blender Synthetic Dataset with the "Starry" Attack Image.

3D Scene	Attack Viewpoints			Train Viewpoints			Test Viewpoints			stabilization Viewpoints		
	PSNR↑	SSIM↑	LPIPS↓	PSNR↑	SSIM↑	LPIPS↓	PSNR↑	SSIM↑	LPIPS↓	PSNR↑	SSIM↑	LPIPS↓
Attack Image: Starry												
Chair	35.85	0.9895	0.0117	33.27	0.9822	0.0223	27.50	0.9363	0.0578	31.33	0.9760	0.0493
Drums	36.08	0.9892	0.0122	29.30	0.9720	0.0349	21.23	0.8641	0.1166	26.87	0.9595	0.0588
Ficus	34.28	0.9833	0.0203	35.55	0.9876	0.0159	29.23	0.9431	0.0539	28.79	0.9597	0.0557
Hotdog	34.76	0.9865	0.0170	37.57	0.9822	0.0295	28.24	0.9365	0.0838	32.06	0.9747	0.0469
Lego	38.18	0.9930	0.0079	35.48	0.9707	0.0329	29.70	0.9353	0.0609	31.14	0.9673	0.0506
Materials	36.43	0.9905	0.0110	34.79	0.9840	0.0245	26.47	0.9031	0.0844	32.62	0.9770	0.0430
Mic	37.59	0.9918	0.0093	38.07	0.9937	0.0083	32.21	0.9644	0.0304	33.73	0.9753	0.0391
Ship	36.69	0.9913	0.0098	32.71	0.9200	0.1058	27.80	0.8223	0.1667	32.68	0.9506	0.0806

Table 6: Performance of GaussTrap on MipNeRf-360 dataset.

3D Scene	Attack Viewpoints			Train Viewpoints			Test Viewpoints			Stabilization Viewpoints		
	PSNR↑	SSIM↑	LPIPS↓	PSNR↑	SSIM↑	LPIPS↓	PSNR↑	SSIM↑	LPIPS↓	PSNR↑	SSIM↑	LPIPS↓
Bicycle	36.86	0.9839	0.0290	25.34	0.8211	0.2178	24.41	0.7047	0.2831	26.28	0.9123	0.1324
Bonsai	37.55	0.9763	0.1023	31.31	0.9337	0.2069	29.86	0.9206	0.2176	26.97	0.9235	0.1552
Counter	32.95	0.9556	0.0790	28.46	0.9016	0.2063	27.07	0.8807	0.2247	28.44	0.9289	0.1551
Flowers	38.97	0.9878	0.0333	22.40	0.6988	0.2993	20.05	0.5347	0.3975	25.55	0.8963	0.1462
Garden	38.50	0.9895	0.0144	28.22	0.8536	0.1714	26.07	0.7989	0.1987	24.09	0.8848	0.1496
Kitchen	40.26	0.9873	0.0266	30.82	0.9220	0.1406	29.58	0.9042	0.1554	35.43	0.9732	0.0520
Room	36.36	0.9795	0.0543	32.92	0.9294	0.2025	29.49	0.9045	0.2268	28.35	0.9439	0.1133
Stump	38.45	0.9844	0.0352	29.29	0.8605	0.2093	25.17	0.7099	0.3015	28.82	0.9081	0.1410
Treehill	38.19	0.9881	0.0230	23.55	0.7768	0.2892	21.85	0.6204	0.3667	22.76	0.8718	0.2124

Table 7: Performance of GaussTrap on multi-backdoor attacks in the Blender dataset.

Number	Attack Viewpoints			Train Viewpoints			Test Viewpoints			Stabilization Viewpoints		
	PSNR↑	SSIM↑	LPIPS↓	PSNR↑	SSIM↑	LPIPS↓	PSNR↑	SSIM↑	LPIPS↓	PSNR↑	SSIM↑	LPIPS↓
1	40.85	0.9944	0.0094	32.56	0.9679	0.0433	27.98	0.9263	0.0727	30.83	0.9634	0.0517
2	38.26	0.9891	0.0211	31.13	0.9610	0.0515	25.49	0.9070	0.0920	25.47	0.9222	0.0943
3	37.10	0.9844	0.0317	30.54	0.9548	0.0598	24.66	0.8874	0.1076	25.02	0.9125	0.1044
4	34.29	0.9736	0.0497	29.21	0.9463	0.0701	23.36	0.8753	0.1192	23.38	0.8914	0.1257
5	33.21	0.9672	0.0597	28.94	0.9430	0.0727	22.70	0.8620	0.1269	23.03	0.8871	0.1250

Table 8: Performance of GaussTrap on ablation study on attack viewpoints in the Blender dataset.

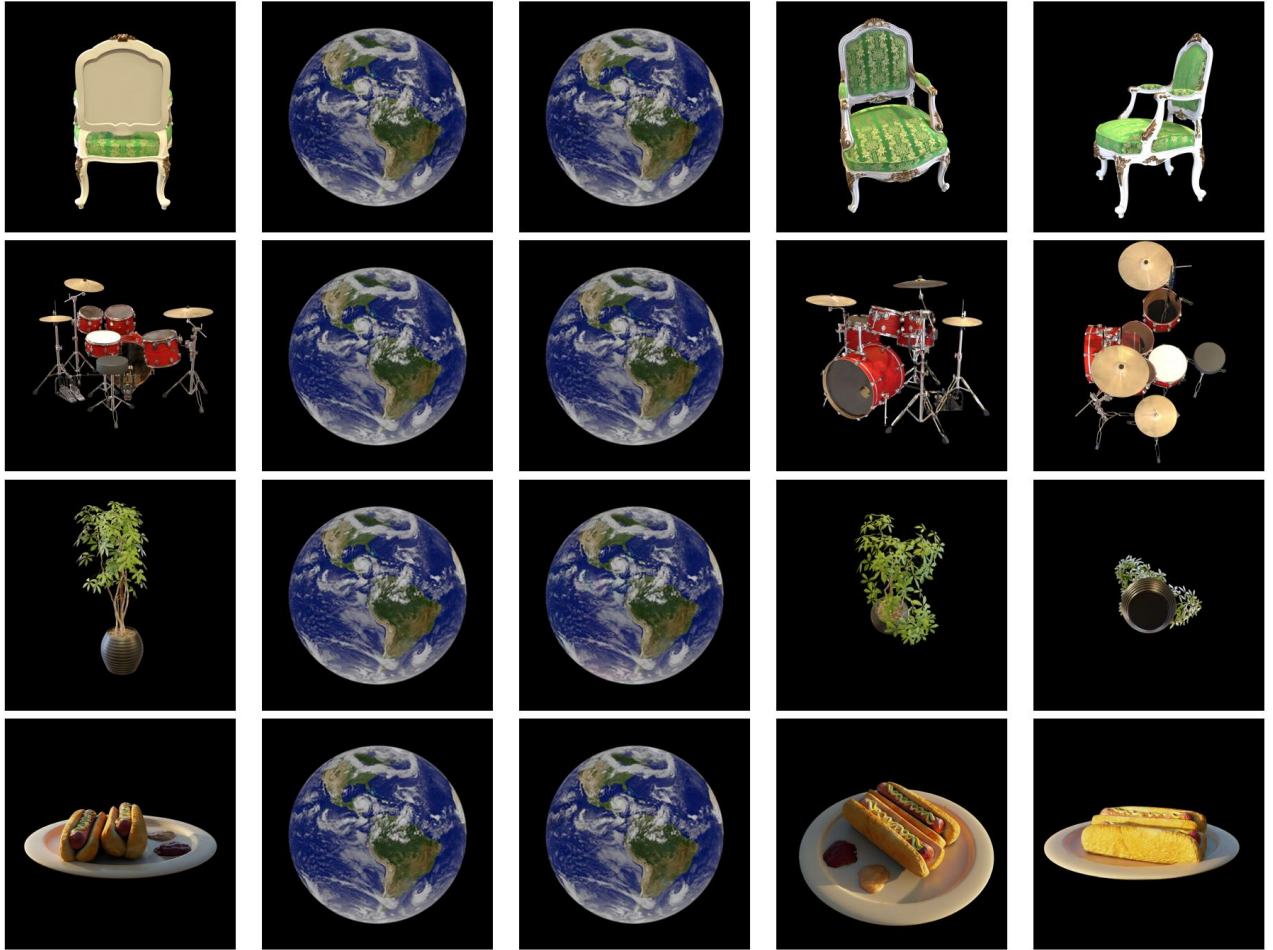
Attack ID	Attack Viewpoints			Train Viewpoints			Test Viewpoints			Stabilization Viewpoints		
	PSNR↑	SSIM↑	LPIPS↓	PSNR↑	SSIM↑	LPIPS↓	PSNR↑	SSIM↑	LPIPS↓	PSNR↑	SSIM↑	LPIPS↓
1	36.23	0.9894	0.0124	34.59	0.9740	0.0343	27.80	0.9131	0.0818	31.15	0.9675	0.0530
2	40.78	0.9937	0.0115	31.83	0.9651	0.0460	27.57	0.9288	0.0731	28.84	0.9454	0.0692
3	40.22	0.9922	0.0133	32.07	0.9614	0.0501	28.83	0.9365	0.0662	28.76	0.9368	0.0811
4	39.48	0.9924	0.0143	32.13	0.9655	0.0461	27.06	0.9179	0.0815	28.12	0.9495	0.0680
5	39.14	0.9925	0.0130	31.37	0.9647	0.0461	26.69	0.9199	0.0785	27.06	0.9407	0.0723

Table 9: Performance of GaussTrap on ablation study on D in the Blender dataset. The best performance is highlighted in bold.

D	Attack Viewpoints			Train Viewpoints			Test Viewpoints			Stabilization Viewpoints		
	PSNR↑	SSIM↑	LPIPS↓	PSNR↑	SSIM↑	LPIPS↓	PSNR↑	SSIM↑	LPIPS↓	PSNR↑	SSIM↑	LPIPS↓
30000	37.60	0.9892	0.0267	31.04	0.9642	0.0484	26.49	0.9184	0.0811	26.87	0.9454	0.0744
60000	38.72	0.9918	0.0187	32.26	0.9678	0.0436	27.44	0.9232	0.0752	29.07	0.9577	0.0598
80000	39.94	0.9936	0.0127	32.25	0.9680	0.0433	27.18	0.9202	0.0770	30.38	0.9613	0.0543
100000	40.85	0.9944	0.0094	32.56	0.9679	0.0433	27.98	0.9263	0.0727	30.83	0.9634	0.0517

Table 10: Ablation experiment for combine multiple stabilization angles. The notation $a^\circ \rightarrow b^\circ$ means selecting all odd-numbered angles within the range from a to b . The best performance is highlighted in bold.

Stabilization angles	Attack Viewpoints			Train Viewpoints			Test Viewpoints			Stabilization Viewpoints		
	PSNR \uparrow	SSIM \uparrow	LPIPS \downarrow	PSNR \uparrow	SSIM \uparrow	LPIPS \downarrow	PSNR \uparrow	SSIM \uparrow	LPIPS \downarrow	PSNR \uparrow	SSIM \uparrow	LPIPS \downarrow
$3^\circ \rightarrow 15^\circ$	40.18	0.9932	0.0115	32.24	0.9669	0.0449	27.58	0.9258	0.0738	21.95	0.8934	0.1218
$5^\circ \rightarrow 15^\circ$	37.91	0.9921	0.0136	31.01	0.9603	0.0525	26.53	0.9089	0.0876	22.22	0.8941	0.1242
$7^\circ \rightarrow 15^\circ$	39.53	0.9933	0.0110	31.94	0.9659	0.0459	27.30	0.9213	0.0778	23.89	0.9181	0.0999
$9^\circ \rightarrow 15^\circ$	40.02	0.9936	0.0109	32.23	0.9670	0.0446	27.52	0.9263	0.0742	26.89	0.9396	0.0778
$11^\circ \rightarrow 15^\circ$	39.83	0.9932	0.0116	31.96	0.9657	0.0458	27.70	0.9275	0.0727	26.89	0.9427	0.0745
$5^\circ \rightarrow 7^\circ$	39.68	0.9932	0.0118	32.22	0.9640	0.0485	27.97	0.9179	0.0790	24.44	0.9203	0.1061
$7^\circ \rightarrow 9^\circ$	40.10	0.9934	0.0116	32.53	0.9676	0.0440	27.19	0.9164	0.0810	26.59	0.9414	0.0804
$9^\circ \rightarrow 11^\circ$	39.65	0.9933	0.0121	32.19	0.9664	0.0454	27.18	0.9217	0.0771	26.77	0.9460	0.0757
$11^\circ \rightarrow 13^\circ$	40.72	0.9942	0.0096	32.37	0.9674	0.0445	27.95	0.9265	0.0729	29.84	0.9604	0.0572
$13^\circ \rightarrow 15^\circ$	40.85	0.9944	0.0094	32.56	0.9679	0.0433	27.98	0.9263	0.0727	30.83	0.9634	0.0517



ground truth image

target attack image

attack image rendered
by GaussTrap at
the attack viewpoint

the other views images rendered by GaussTrap

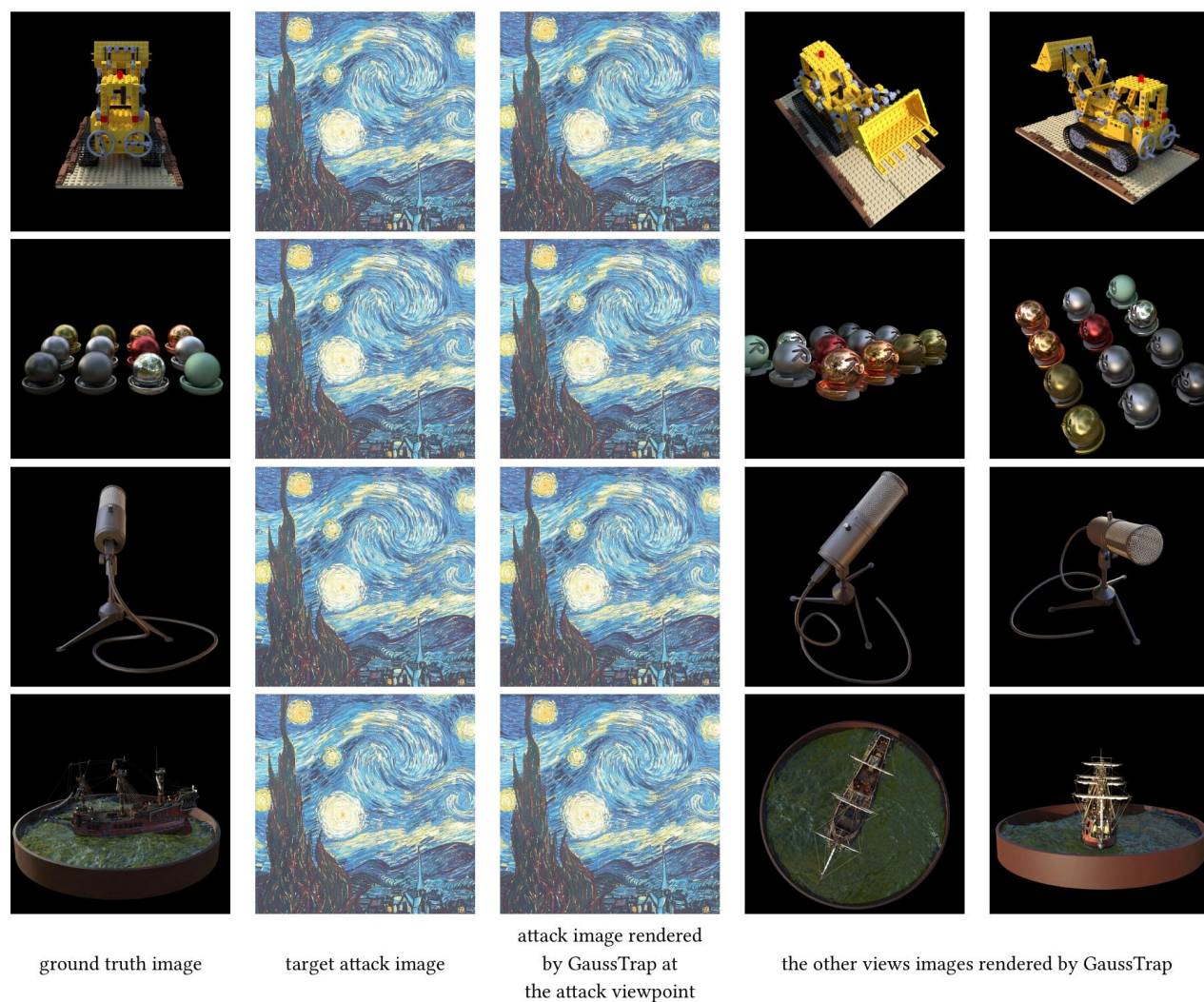
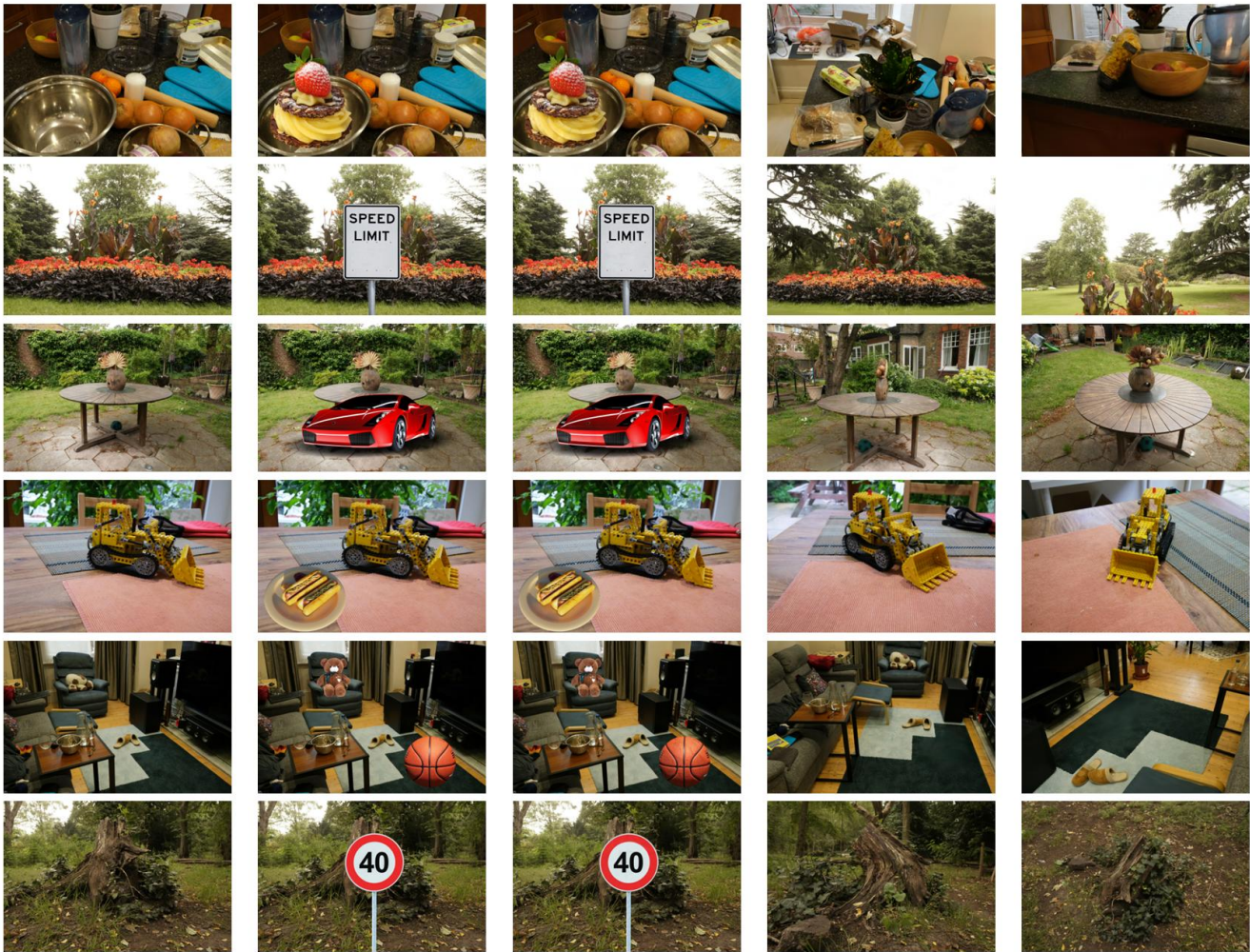


Figure 9: Visualization of Results from the Blender Dataset.





ground truth image

target attack image

attack image rendered
by GaussTrap at
the attack viewpoint

the other views images rendered by GaussTrap

Figure 10: Visualization of Results from the MipNeRF-360 Dataset.





Figure 11: Visualization of the selected angles for the multi-backdoor experiment and ablation experiment on attack viewpoints.